Characterization of particulate matter emitted by a marine engine operated with liquefied natural gas and diesel fuels

Corbin, Joel C.; Peng, Weihan; Yang, Jiacheng; Sommer, David E.; Trivanovic, Una; Kirchen, Patrick; Miller, J. Wayne; Rogak, Steven; Cocker, David R.; Smallwood, Gregory J.; Lobo, Prem; Gagné, Stéphanie

Publisher's version / Version de l'éditeur:
https://doi.org/10.1016/j.atmosenv.2019.117030
Atmospheric Environment, 2019-10-09

Characterization of particulate matter emitted by a marine engine operated on liquefied natural gas and diesel fuels

Joel C. Corbin*[a], Weihan Peng[b], Jiacheng Yang[b], David E. Sommer[d], Una Trivanovic[d], Patrick Kirchen[d], J. Wayne Miller[b,c], Steven Rogak[d], David R. Cocker[b,c], Gregory J. Smallwood[a], Prem Lobo[a], Stéphanie Gagné*[a]

[a] *Metrology Research Centre, National Research Council Canada, 1200 Montreal Road, Ottawa, Ontario K1A 0R6, Canada*
[b] *Center for Environmental Research & Technology, University of California Riverside, 1084 Columbia Ave, Riverside, 92507 CA, USA*
[c] *Chemical and Environmental Engineering, University of California Riverside, 1084 Columbia Ave, Riverside, 92507 CA, USA*
[d] *Department of Mechanical Engineering, University of British Columbia, 2054-6250 Applied Science Lane, Vancouver, BC V6T 1Z4, Canada*

Abstract

Liquefied natural gas (LNG) is becoming increasingly popular as a marine fuel as emission regulations become more stringent. However, very little data are available on the particulate matter emissions of modern marine natural gas engines. In this study, we present a first detailed characterization of the composition of the particulate matter emitted by a modern, in-use, natural-gas-powered vessel. The vessel engines use compression-ignition and only a small amount of diesel fuel as pilot. Our emissions characterization includes six different techniques to measure black carbon, including all methods determined as appropriate for measuring BC emissions from ships by the International Maritime Organization, as well as particle size distributions, metal concentrations, and organic particulate emissions. Particulate-matter emissions differed significantly between idle and at-sea operating conditions. At idle, particulate emission factors were primarily organic (approximately 1500 mg/kWh), with black carbon emission factors over two orders of magnitude lower (5.6 ± 0.4 mg/kWh). At engine loads above 25%, all emissions were independent of load and substantially lower than at idle, at 4.4 ± 1.7 mg/kWh for organics and 0.8 ± 0.2 mg/kWh for black carbon. When operated only on diesel fuel, this engine emitted 8-fold more organic particulate matter (38 ± 15 mg/kWh) and 37-fold more black carbon (30 ± 11 mg/kWh) at loads above 25%. At idle loads, the diesel-fuel emissions were comparable to the natural-gas emissions. In addition to organics and black carbon, a third category of non-volatile sub-10-nm particles was identified. A detailed consideration of our measurements indicated that the sources of the organic, BC, and sub-10-nm particles were lubrication oil, diesel pilot fuel, and lubrication-oil metals, respectively. Future studies should seek to quantify the emissions of other dual-fuel engines that will be entering the market.

Highlights

- Detailed characterization of particulate matter emissions from natural-gas-powered marine vessel.
- Particulate mass and number was primarily volatile organics, which may originate from lubrication oil.
- Black-carbon emissions were a factor 37 higher when using diesel fuel compared to liquid natural gas fuel.

Keywords. LNG; natural gas; marine; particulate matter; diesel; lubrication oil

Email addresses: Joel.Corbin@nrc-cnrc.gc.ca (Joel C. Corbin*), Stephanie.Gagne@nrc-cnrc.gc.ca (Stéphanie Gagné*)

1. Introduction

Marine transportation is traditionally powered by non-renewable crude-oil fossil fuels, either residual or distillate, the availability of which is fundamentally limited [1]. Partly for this reason, attention has recently shifted to natural gas (NG), a mixture of gaseous fossil fuels typically containing approximately 90% methane, a small percentage of ethane, and traces of other alkanes and nitrogen [1], which may be transported and used as liquefied NG (LNG). A far more urgent reason is the goal of reducing CO_2 emissions by at least 50% by 2050 in order to stabilize the climate [2, 3]. NG is considered to have the potential to contribute to such reductions because its low carbon-to-hydrogen ratio results in fewer moles of CO_2 produced per mole of NG combusted relative to heavier fossil fuels, and its lower heating value is slightly higher than that of gasoline or diesel [1, 3]. In the longer term, a transition from NG to sustainable biogas fuels may also be preferable to a transition from diesel to sustainable biodiesel [4, 5].

For sufficiently-rich combustion mixtures [6], NG combustion produces substantially lower concentrations of particulate matter (PM) than traditional fuels [1]. This is because of its low number of carbon atoms per molecule, as well as its low carbon-to-hydrogen ratio [7]. The low carbon-to-hydrogen ratio of NG therefore reduces both its PM and its CO_2 emissions. Similarly, NG combustion also emits smaller amounts of nitrogen oxides (NO_x) than traditional fuels due to its lower combustion temperatures. However, emissions of carbon monoxide (CO) and of total volatile hydrocarbons (TVHCs), particularly methane, tend to be higher for NG than for traditional fuels [1]. The mixture of gas-phase and PM pollutants emitted by NG combustion can therefore be expected to be substantially different to the emissions from traditional fuels. This is likely to result in a substantially different toxicity, as indicated by the very different biological effects observed between traditional fuels such as diesel and heavy fuel oil which have been observed on human lung cells [8].

In addition to their harmful effects on public health, combustion emissions may adversely affect the environment through radiative forcing of the climate, deposition on snow, and potentially eutrophication or acidification [5, 9]. The radiative forcing exerted by greenhouse gases such as CO_2 and methane generally act on a global scale, as the atmospheric lifetime of these gases ($\gg 200$ [10] and 10 years [11], respectively) is much longer than the 1–2 years they require to be mixed throughout the tropo- and stratospheres [11]. In contrast, PM exerts a regional radiative forcing as it has a short lifetime of only 1–2 weeks before being deposited to the surface [11]. If deposited onto snow, light-absorbing PM such as black carbon (BC) may continue to exert a radiative forcing [12, 13, 14]. The greater sensitivity of the Arctic to BC deposition is particularly noteworthy, as the Arctic currently faces substantial increases in marine traffic in upcoming decades due to retreating sea ice[15], which has motivated ongoing discussions at the International Maritime Organization (IMO) to investigate BC emissions from marine vessels. Other regional effects of BC may include the formation [16] or induced-evaporation of clouds [17].

The cetane number of NG is so low that it is not usually quoted [1], meaning that compression-ignition engines require a pilot fuel, such as diesel, to initiate combustion. The percentage contribution of this pilot fuel to the total fuel energy is typically about 30% [1], but is as low as 1% in modern marine NG engines such as the one studied herein. It is therefore not clear to what degree the results of previous studies on NG combustion [1, 18, 19, 20, 21, 22, 23] are relevant to such NG engines. Moreover, there is a need for a more comprehensive emissions characterization of dual-fuel engines, as the following summary of existing NG studies on either buses or marine vessels will demonstrate.

Almost no information is available on the properties of the PM emitted by LNG-powered marine engines. The only published peer-reviewed study is that of Anderson et al. [24]. Anderson et al. [24] characterized particle number and gaseous emissions from a compression-ignition, LNG-powered ship and found that particles

were generally volatile, with mobility diameters < 50 nm after 20-fold dilution. Consistent with general trends for NG [1], CO and total gas-phase hydrocarbons (HCs, as measured by flame ionization) emissions were higher for NG than diesel-fuel operation. In contrast, PM number, NO_x, SO_2, and CO_2 were lower for NG. PM mass, as estimated from Engine Exhaust Particle Sizer (EEPS) measurements, was also lower. However, as noted by those authors, the EEPS is not an accurate technique and requires several empirical corrections in order to be reliable, which could not be made in their study. Finally, based on the trace-metal content of the PM, Anderson et al. [24] hypothesized that the volatile fraction of NG-combustion PM originated from evaporated lubrication oil, and that the non-volatile fraction originated from metal oxides within the oil.

No other studies have measured the emissions of NG-powered ships, although recent studies on NG-powered buses are worth mentioning in the present context [23]. These studies have generally concluded that the PM from NG combustion is largely volatile, and that methane and other HCs respectively represent the greatest risk to climate and public health from NG emissions. The introduction of a catalyst into the exhaust of an NG engine has been shown to reduce those HC emissions by a factor of 20 to 50, with a corresponding 20-30 fold reduction in genotoxic activity [25]. Reliable measurements of black carbon (BC) concentrations from NG combustion have not been reported to our knowledge.

Here, we have performed a detailed characterization of the aerosol emitted by a dual-fuel engine primarily combusting NG for the propulsion of a commercial, in-use vessel. Our characterization focusses on the PM emissions, in particular, on quantifying the amounts of BC and organic carbon (OC) observed at different engine loads. We discuss volatile and non-volatile particle size distributions, the physical origin of BC and OC, the relative performance of various techniques used to measure BC, and the importance of these PM emissions in the context of co-emitted methane and HCs. Recommendations for the future use of NG engines are provided.

2. Methods

Measurements were taken aboard a commercial, in use NG-powered vessel in western Canada. The vessel is powered by two nine-cylinder, compression-ignition, dual-fuel, four-stroke diesel engines with a power output of 4320 kW each. The engine has been in use for less than a decade. While the vessel stores its fuel as LNG, we refer to the fuel as NG where appropriate since the fuel is injected in gaseous form as NG. The NG is indirectly injected and ignited by a diesel-fuel pilot charge, which contributes $< 10\%$ of the total derived energy at 10% engine load, and much less at higher loads. The diesel pilot fuel is injected by a common rail system. The engines operate at constant speed and varying load to drive electrical generators. The engines are specifically designed for operation on NG, rather than being retrofitted, and are also capable of running entirely on diesel fuel. The engine meets Tier 3 emission standards in NG mode and Tier 2 standards in diesel mode.

The measurements presented herein were taken on a single engine during normal operation of the vessel. The load of the engine was set to a desired value between 6 and 91% of the rated maximum of 4320 kW (Table 1), typically for 30 minutes, while any additional required power was provided by the second engine. The actual time spent at each load during commercial operation can be varied by the operator, as discussed further in Sommer et al. [6]. Both LNG (91–95% methane) and ultra-low-sulfur diesel fuels were used. The vessel normally operates with LNG.

The engine emissions were extracted from the exhaust stack at average temperatures above 350 °C, using the sampling configuration shown in Figure S1. Three lines distributed the sample to multiple instruments, as summarized in Table 2. The first two lines were used by an AVL 415SE smoke meter (AVL LIST GmbH,

Austria) and a Horiba PG350 portable gas analyzer (Horiba, Japan). The third line was heated to 50–60 °C, connected to a sampling manifold of the design described in Gysel et al.[26], diluted approximately sixfold with compressed, dried and activated-charcoal-filtered air, and then distributed to the remaining instruments. The total sampled flow (approximately 60 L min^{-1}) was less than the total available flow, and an excess flow of approximately 10 L min^{-1} was directed into an exhaust line. The dilution factor was determined as the ratio of background-subtracted CO_2 concentrations before and after dilution; the measured background CO_2 concentration was 454 ± 12 ppmv (mean ± SEM of multiple background measurements). The sampling line length between manifold and instruments (2 to 4 m) was selected to give approximately comparable residence times of 2 to 4 seconds in each case.

The remaining instruments included five BC instruments (described below), a scanning mobility particle sizer (SMPS, TSI, USA), two sets of filter samplers, two transmission electron microscopy samplers, a custom-built methane sensor, a CO_2 monitor, and a flame ionization detector for methane and non-methane HCs. The filter samplers were used to obtain quartz-backed-quartz and teflon samples for thermal–optical carbon analysis (TOA; EUSAAR2 protocol [27]) and X-ray fluorescence spectroscopy (XRF) analysis, respectively. The filters which were analyzed by TOA were sealed and stored on ice prior to their measurement. The TEM samples were collected in duplicate using using two different samplers, a thermophoretic sampler constructed at the University of British Columbia and an electrostatic sampler (ESPnano, DASH Inc., USA) [28], and were analyzed using a Hitachi H7600 at 80 eV acceleration voltage; a detailed analysis will be presented elsewhere (Trivanovic et al., in review). The custom-built methane sensor utilized wavelength modulation spectroscopy and was validated in the laboratory as described by Sommer et al. [6].

The SMPS (TSI model numbers 3088, 3082, 3081 and 3776) employed an X-ray charger and generally scanned the mobility-diameter range 6–170 nm. The SMPS data were monitored throughout the experiments and, when evidence of larger particles was present, the upper limit of the SMPS scans was extended to ensure that the majority of particles had been observed (in number space). A median SMPS scan time of 20 seconds was used; scans of up to 200 seconds were used to ensure that 20 seconds was adequately long. The SMPS was used to obtain number-based particle size distributions and to estimate concentrations of both total PM (after the factor of approximately 6 dilution) and non-volatile PM. Non-volatile PM was obtained after denuding at 623 K using a catalytic stripper (Catalytic Instruments GmbH, Germany, model CS015). The SMPS estimations of total PM mass are approximations, as the instrument is designed to measure number rather than mass. The more reliable measurement of total PM mass in this study was obtained from the carbon mass measured on the filters by thermal–optical analysis (TOA), as described below.

2.1. BC (eBC, rBC, and EC) measurements

Motivated by ongoing discussions at the IMO on measurement of BC and the investigation of BC control measures in the context of marine emissions in the Arctic, we deployed multiple instruments to measure BC during this campaign. BC is a complex material which is normally defined as consisting of aggregates of nano-spherules of refractory, insoluble, strongly-light-absorbing, sp^2-bonded graphitic carbon [29, 30]. The preceding list of properties means that different measurement principles may be used to determine BC mass concentrations. In the following, we follow the recommendations of Petzold et al. [29] and use technique-specific terminology when discussing the measurements of different BC instruments. The properties of the instruments described in this section are summarized in Table 2.

It is essential to note that some types of PM may possess properties (in terms of solubility, light absorptivity, refractoriness, and sp^2 bonding) which overlap with the above-mentioned defining properties of BC [31]. Since most BC measurement instruments rely on measuring only one of these properties, disagreement

between different BC measurements may result in special cases of complex PM mixtures. In particular, for engines operated on heavy fuel oil, the presence of so-called tar and char PM will result in disagreement between instruments which aim to exploit either the light absorption, refractoriness, insolubility, or sp^2 bonding of BC [31]. (The only other special case is that of biomass-burning PM [31].) The principles on which these instruments operate are defined in the following.

The most common measurand for BC is light absorption at a wavelength λ, which may be reported as equivalent BC concentrations eBC(λ) if a mass-specific absorption efficiency (MAE) is assumed [32]. In this study, the Photoacoustic Extinctiometer [PAX; Droplet Measurement Technologies, USA; eBC(870 nm)] [33], CAPS PMssa monitor [Aerodyne Research Inc., USA; eBC(660 nm)] [34], Micro Soot Sensor [MSS, AVL GmbH Austria; eBC(808 nm)] [35], and smoke meter [eBC(560 nm)] [36] all measured and reported eBC assuming the MAE of 7.5 $m^2 g^{-1}$ at $\lambda = 550$ nm recommended by Bond et al. [37]. For each instrument, this MAE is converted to the measurement wavelength by assuming a wavelength-independent refractive index, from which it follows [38] that $\mathrm{MAE}(\lambda_i) = \mathrm{MAE}(550\,\mathrm{nm}) \cdot 550\,\mathrm{nm}/\lambda_i$.

The eBC instruments were calibrated as follows. The scattering detectors of the PAX and CAPS were calibrated on-site using non-absorbing aerosol (ammonium sulfate), according to the manufacturer's instructions. The absorption coefficient of the PAX was additionally calibrated with nebulized Aquadag (colloidal graphite). The MSS and smoke meter were not calibrated on-site. The MSS is calibrated against EC (defined below), although its principle of operation is identical to the PAX. The smoke meter measures the attenuation of green light ($\lambda = 560$ nm) through a PM-laden filter and reports filter smoke numbers (FSN), which were converted to eBC concentrations by the instrument software using the manufacturer's calibration (provided in the supplement as Equation S1).

Two other BC measurement techniques were employed. First, laser-induced incandescence (LII) was employed by the Artium LII-300 (Artium Technologies, CA, USA). This involves heating particles to approximately 3000 K with a high-fluence laser and measuring the intensity of laser-induced incandescence (LII) that results. From this intensity measurement, together with a two-colour-pyrometry measurement of temperature and literature knowledge of the BC absorption function $E(m)$, a measurement of BC known as refractory BC (rBC) [29] can be retrieved as a mass concentration. The LII detectors are calibrated with a spectral radiance standard and the overall rBC quantification is calibrated against EC, as described by Snelling et al. [39].

Second, thermal–optical analysis (TOA) was employed for the quartz-fibre filters, using a bench-top Sunset analyzer (Model V5) calibrated with sucrose and following the EUSAAR2 protocol, which is designed to minimize potential artifacts [27]. Filter punches (area 1 cm^2) were first heated in helium to desorb volatile carbon (the so-called organic carbon or OC mass) before the remaining carbon residue (the so-called elemental carbon or EC mass) was combusted in 2% oxygen. Because some OC may pyrolyze during analysis, transmittance (and reflectance) of a 630 nm laser through the filter punch is monitored throughout. In this study, pyrolysis was observed to be negligible in general.

When analyzing a first filter taken during NG operation at engine-idle conditions, we observed that the OC concentrations were extremely high and resulted in saturation of the TOA analyzer detectors. This occurred because filter sampling times were calculated according to the desired BC concentration, rather than the OC concentration. We therefore performed two separate experiments to determine OC concentrations at idle. First, we performed an isopropanol extraction of an idle-load filter before performing EUSAAR2 analysis, and found that the results were in excellent agreement with the consensus value discussed below. Second, we modified the EUSAAR2 protocol by adding an additional, slower heating step between the first

and second stages of helium-atmosphere desorption in order to quantify carbon on these filters. This second experiment was performed to avoid detector saturation and allowed us to quantify OC concentrations at idle by subtracting the total evolved carbon from the EC determined from the extraction, as recommended by the VDI 2465/1 protocol [40].

The OC concentrations at idle were also estimated using the SMPS data. At idle, the uncertainties associated with estimating mass from SMPS measurements were lowest, since the single scattering albedo (ratio of scattering to extinction coefficients) measured by the CAPS PMssa showed that a large fraction of the PM mass was OC, reducing the uncertainty associated with the assumption that particles were spherical. However, agreement between SMPS and OC at idle was still poor (Figure S6) and we rely on the SMPS-estimated mass below for qualitative interpretation only.

2.2. Calculated quantities

Engine emission factors $\mathrm{EF_m}$, in terms of PM mass emitted per kWh produced, were calculated as

$$\mathrm{EF_m} = \frac{[\mathrm{PM}]_\mathrm{m} \cdot Q_\mathrm{exhaust}}{P} \tag{1}$$

Where $[\mathrm{PM}]_\mathrm{m}$ is the mass concentration of a PM species in $\mathrm{mg\,Nm^{-3}}$, Q_exhaust is the engine exhaust flow rate (measured in-situ for a given test point with a pitot probe) in $\mathrm{Nm^3\,h^{-1}}$, and P is the engine power in kW reported by the engine control software. All concentrations were corrected to standard conditions of 273 K and 1 atmosphere.

Equation 1 can also be used to calculate number-based EFs, if the quantity $[\mathrm{PM}]_\mathrm{m}$ is replaced by $10^6\,[\mathrm{PM}]_\mathrm{n}$, with $[\mathrm{PM}]_\mathrm{n}$ given in units of particles per $\mathrm{cm^3}$.

Measured size distributions were corrected for losses in the catalytic stripper by multiplying the measured values with a penetration function provided by the manufacturer, which was itself derived through a combination of theory and empiricism (personal communication, Catalytic Instruments, 2018).

Particle penetration through our sampling system was modelled using the software published by von der Weiden et al.[41]. At 10, 20, 40, 100 nm penetration to the SMPS was 73, 85, 91, 95 %. The size-resolved penetration is shown in Figure S4 in the context of the particle volume distribution calculated from the SMPS data for each engine load. Comparison of the penetration function and volume distribution shows that the majority of BC (largest mode) will have been measured with approximately 95% penetration, whereas OC will have been measured with approximately 75% penetration and the small involatile mode discussed below will have been measured with approximately 60% penetration. We have not corrected the values reported below by these penetration estimates.

No loss correction for the remainder of the sampling lines was made. As there were no small-angle bends in that sampling line, such losses would be dominated by diffusion to the tubing walls, which (for $5\,\mathrm{L\,min^{-1}}$ flowing through 2.5 m of tubing) fall from 99% at approximately 100 nm mobility diameter to 50% at about 20 nm and 20% at about 11 nm [42]. The corresponding losses of the smallest mode of particles measured below 20 nm would therefore be substantial. However, as our sampling system was not designed to quantify such particles, we have not attempted to perform a correction.

2.3. Uncertainties

In general, error bars are reported as the standard error of the mean (SEM, representing variability in the specific measurement point). Mean values (such as emission factors) are reported together with their standard deviations (representing the spread of measured values).

When calibration uncertainties were analytically available (CAPS, PAX, CO_2 monitor) they were added in quadrature to the statistical imprecision, as described in the following. The span value of the CO_2 monitor was checked at the beginning and end of each day using a 14.42% CO_2 reference mixture; the measured value was always within ±2% of the reference value. This ±2% was therefore propagated into the CO_2 uncertainty. (No absolute-value CO_2 uncertainty is necessary, since all measurements were of high CO_2 concentrations [43].) The CAPS calibration results in a single scattering-coefficient calibration factor, which is obtained by the slope of a weighted least-squares fit; the corresponding uncertainty in the fitted slope was propagated into the uncertainties reported here. The PAX calibration results in an analogous slope and a similar procedure was applied. As no other instruments were calibrated on-site, no other calibration uncertainties were treated explicitly. Overall, statistical uncertainties were generally smaller than the symbols in the plots shown below, with the exception of some SMPS data. Unquantified uncertainties, such as the potential measurement biases between BC instruments, are considered qualitatively by comparing instruments when possible.

Special uncertainties are worth mentioning for certain instruments. In general, the quantities presented below were measured analytically. The exception is the SMPS-estimated mass concentration, which was estimated by treating all measured particles as spheres with an assumed effective density. This density is described as effective because it requires the assumption of particle sphericity. Previous studies[44, 45] have measured the effective density of typical BC particles in the size range discussed below as 700–900 $\mathrm{kg\,m^{-3}}$. For an NG-powered engine, Bullock and Olfert[18] reported a mean effective density of 850 $\mathrm{kg\,m^{-3}}$ under conditions where > 95% of the PM was volatile. Bullock and Olfert also reported that this density is similar to that of lubrication oil. Here, we have used an effective density of 850 $\mathrm{kg\,m^{-3}}$ for all engine conditions, which serendipitously applies to both OC and BC particles, according to the discussion above. We note that the uncertainty of this effective density is greatest for BC, and estimate a 25% uncertainty in the accuracy of all SMPS-derived mass concentrations. The corresponding error bars shown below do not include this 25% and reflect statistical variability only.

Table 1 about here; instrument descriptions.

3. Results

3.1. Overview of NG-mode engine emissions

Figure 1 about here; a simple example of our data set.

A typical time series of the engine output is shown in Figure 1. The figures shows a period of rapid changes in engine load as the vessel was manoeuvred close to shore. This time period was selected to highlight several features of the engine: stable emissions at engine loads above 20%, variable BC concentrations at lower engines loads, and the emission of substantial amounts of volatile PM at lower engine loads.

The increase in variability of BC concentrations at lower engine loads in Figure 1 is shown by all four real-time BC instruments (CAPS, LII-300, MSS, and PAX). This variability corresponds to the triggering of a cylinder-deactivation strategy by the engine-control software at engine loads below 15 %. This cylinder-deactivation strategy entails deactivating LNG injection to two of the nine engine cylinders to increase combustion efficiency and therefore substantially reduce methane emissions [6]. Diesel pilot fuel is still injected in all cylinders.

A substantial increase in volatile PM emissions was observed at lower engine loads, as evident from the SMPS data shown in Figure 1. The figure shows the integrals of the first (number) and third (volume)

moments of the SMPS size distributions, labelled as $N_{6\text{-}170\text{nm}}$ and (after weighting by an effective density of 850 kg m^{-3}) mass concentration. It is clear that the total PM mass increases substantially immediately after the engine load fell below approximately 15%, As discussed further below, this increase in PM mass is attributable to organic PM, since BC concentrations remained constant and the LNG fuel is sulfur-free.

3.2. Size distributions and TEM of volatile and non-volatile particles

Figure 3 about here; Size distributions vs load for NG showing volatile and nonvolatile PM.

Figure 2 about here; TEM images.

Figure 2a shows the mobility-size number distributions measured at various loads for LNG-mode operation. The number distributions are generally log-normal with a mode diameter of 10–20 nm at engine loads $\geq$ 30 %, and 50 nm at 6% load (idle) load. Repeated measurements at higher loads indicated a substantial variability in mode diameter, which is discussed further in Section 4 below. Figure 2b shows that the primary particle mode at 50% load evaporated upon heating to 623 K; this 10–20 nm mode was therefore composed of organic PM and not BC.

The larger non-volatile particles shown in Figure 2b were typical soot aggregates, as shown by the TEM micrographs presented in Figure 3a-c. These examples were selected to be representative of a detailed TEM analysis which is to be published in a separate manuscript (Trivanovic et al., in review). Note that the TEM images do not include the most abundant particles in the PM, which dominate the particle number distributions in Figure 2a, because those particles were volatile.

The TEM images also do not represent the extremely small ($<$ 10 nm) non-volatile particles visible in Figure 2b. These particles remained visible after heating to 623 K, and were not partially-evaporated organics: their size did not grow when the heating temperature was reduced from 623 K to either 473 or 548 K (Figure S2). We therefore hypothesize that these particles consisted of nucleated metal-oxides [46] from the lubrication oil.

We emphasize that the measured mass (and size) of organic PM is a function of the amount of dilution employed prior to its measurement [47, 48]. Correspondingly, the larger particles measured at 6% load should be interpreted as caused by the higher overall organic PM mass concentrations. The potential cause of these higher organic emissions at lower load is discussed further in Section 4. Particle volume distributions corresponding to Figure 2a are shown in Figure S4.

When operating the engine with diesel fuel, the particle size distribution was substantially larger and bimodal, corresponding to the emission of BC-dominated rather than organic-dominated PM. Figure 2b shows the diesel-fuel size distributions at 50% load, for total and non-volatile particles; Figure S5 shows the distributions at all loads. The smaller mode was volatile, and corresponded to organic PM, whereas the larger mode was non-volatile, corresponding to BC.

3.3. Number, BC, and OC emission factors

Figure 4 about here; (a) PM emission factors vs load.

Figure 4a shows the measured emission factors, per kWh, of the present engine in NG mode. The BC- and number-based emission factors were constant for loads above idle. Organic PM emissions were greater than BC emissions, at 4.4 $\pm$ 1.7 mg/kWh (mean $\pm$ SD) for organic PM compared to 0.8 $\pm$ 0.2 mg/kWh for BC. However, the BC particles were much larger than the organic particles, such that light scattering from the organic PM was relatively minor and the aerosol SSA at 660 nm was generally dominated by BC; the

measured SSA of approximately 0.2 (Figure 5) at higher loads is consistent with literature values for BC-only aerosols [37]. At lower loads, this SSA was as high as 0.5, due to the correspondingly larger size of organic PM (Figure 2a).

Figure 5 about here; single-scattering albedo data.

Figure 4b shows the same data as Figure 4a for diesel-powered operation. Switching from LNG to diesel mode, the BC emission factors at higher loads increased by over an order of magnitude, from 0.8 ± 0.2 to 30 ± 11 mg / kWh (mean and relative standard deviation of all BC measurements for $\geq 30\%$ load). Idle emissions of BC were not changed by fuel switching, and were 5.6 ± 0.6 mg/kWh in both LNG and diesel modes. Idle emissions of organic PM were extremely high in both modes, (1450 ± 75 and 518 ± 28 mg/kWh in LNG and diesel modes respectively) as shown in Figure 4b. At higher loads, particle number emissions were somewhat higher in LNG mode ($(6.9 \pm 2.7)\, 10^{13}\,\mathrm{kWh}^{-1}$) compared to diesel mode ($(3.8 \pm 1.7)\, 10^{13}\,\mathrm{kWh}^{-1}$). In both cases, these values were an order of magnitude higher at idle ($(3.8 \pm 0.2)\, 10^{14}\,\mathrm{kWh}^{-1}$ for LNG mode, $(3.3 \pm 0.3) 10^{14}\,\mathrm{kWh}^{-1}$ for diesel mode), due to the higher OC emissions. SSA measurements for diesel mode were not available as the BC concentrations were above the upper limit measurable with the CAPS $\mathrm{PM_{SSA}}$ at the dilution levels employed herein.

3.4. Consistency between BC measurements

A major goal of the present study was to investigate to what extent different techniques for measuring BC would be reproducible for LNG-mode emissions. The very small scatter between BC instruments in Figure 4a shows that all instruments performed consistently. The similarity in scatter between Figure 4a and Figure 4b indicates that the performance under LNG- and diesel-modes was comparable, in spite of a factor 50 higher BC concentrations in diesel mode. Figure S3 allows a more detailed comparison of the instrument performances by plotting the ratio of each instrument to an arbitrary reference instrument as a function of BC mass concentration. These ratios were generally within the range $\pm 20\%$, with two exceptions: the ratio for the AVL 415SE Smoke Meter increased to approximately2 at mass concentrations below $30\,\mu\mathrm{g\,m}^{-3}$; and the ratio for the CAPS $\mathrm{PM_{SSA}}$ became meaningless at mass concentrations above $800\,\mu\mathrm{g\,m}^{-3}$, as this instrument is not capable of measuring such high concentrations. The lower detection limit of the Smoke Meter, according to its manual, is $20\,\mu\mathrm{g\,m}^{-3}$. While in our data set, the instrument accuracy suffered at concentrations slightly above this limit, we also note that the instrument accumulates PM prior to each measurement, so that a change of sampling configuration could improve its accuracy at lower concentrations, in future work.

4. Discussion

4.1. Comparison with literature

Data on the emissions of LNG marine vessels are very scarce in the literature. To our knowledge, the only study of this nature is that of Anderson et al. [24]. The engine studied by Anderson et al. [24] (Wärtsilä 8L 50 DF) was slower (514 rpm) than the engine we studied herein (720 rpm), with a longer bore and stroke (500 and 580 mm) than the engine we studied (340 and 400 mm). Its maximum mechanical output is 15,600 kW, compared with 4,320 kW for the engine we studied.

Anderson et al. [24] reported number emission factors that were independent of load, for loads above 30%, with a mean value of approximately $5 \times 10^{12}\,\mathrm{kWh}^{-1}$, over two orders of magnitude lower than our corresponding mean and standard deviation of $(4.4 \pm 1.7) \times 10^{14}\,\mathrm{kWh}^{-1}$. Note that although our measured

size range, 6–170 nm, was smaller than theirs, 5.6–560 nm, the measured size distributions in both cases indicate that the instruments counted the majority of particles.

Anderson et al. also estimated non-volatile PM mass emission factors from these number-distribution measurements at $> 30\,\%$ load as approximately 0.15 mg/kWh, substantially smaller than our corresponding value of 0.79 ± 0.17 mg/kWh. We consider this difference as much greater than the uncertainty in the data sets. Overall, the emission-factor differences between the engine studied by Anderson et al. [24] and the engine we studied highlight the extent to which emission factors may vary with engine design parameters.

4.2. Origin of PM emissions in NG mode

In NG mode, both BC (Figure 4) and CO_2 (Figure S7) emission factors were constant as a function of engine load, for loads $\geq 30\%$. At lower engine loads, decreased combustion efficiency has been highlighted as leading to methane emissions due to a decreased burnoff of injected methane [6]. Our data show that this decreased combustion efficiency also corresponds to enhanced emissions of organic PM and BC. These enhanced emissions may be attributed to a decreased burn-off of the PM, as predicted by theory [1].

Figure 6 about here; effects of skipping methane injection.

BC emissions were constant at all other loads, which leads to the hypothesis that the primary source of BC was the diesel-fuel pilot injection. We tested this hypothesis by considering an experiment in which the number of deactivated cylinders under idle conditions was varied. As shown in Figure 6, either two (the default number during this study), zero, or three cylinders were deactivated. Each cylinder was deactivated for a short time period only, as controlled by the engine software. The figure shows that injecting NG into all cylinders (middle case) resulted in lower BC emissions than deactivating NG injection into two or three cylinders. In other words, BC emissions increased when increasing the ratio of diesel to NG fuel in the cylinders. The observed near-instantaneous decrease in BC suggests that the diesel pilot fuel serves as a source of BC whereas the NG serves as an overall sink by increasing burnoff. We assume here that potential differences in fuel injection timing during cylinder deactivation conditions were negligible; we did not have access to this information in this study.

Deactivating three cylinders instead of two led to slightly more BC. Also, BC concentrations were more variable during cylinder deactivation, on a timescale of seconds. Since cylinder deactivation involved rapidly switching which two or three cylinders were deactivated, this variability indicates that the switching process directly influenced BC emissions. Variability in the organic PM emissions occurred on a different timescale. Rather than a rapid variation, a slow decrease on a timescale of several minutes is observed in Figure 6 after a change in cylinder deactivation strategy. This slow decrease indicates that the organic PM did not originate directly from the NG but from some mechanism associated with the engine operation or equilibration, such as the evaporation of lubrication oil.

Organic PM emissions at lower loads were an order of magnitude greater than BC emissions for both diesel- and LNG-mode operation, in terms of mass-based emission factors. These emissions were almost negligible at higher engine loads (Figure 4 and Figure 5) for both NG and diesel mode. These condensed-phase organics therefore likely originated from lubrication oil, based on their independence from NG injection (Figure 6), the similar patterns of organic PM emissions between the two fuel modes, the observed volatility of the organic PM (Figures 2 and S2), and the literature evidence [18] of the organic PM density being similar to that of lubrication oil. However, we emphasize that gas-phase organic emissions of methane (Figures S7 and S8) were substantial..

Finally, our data show that BC and organics are not the only PM found in the NG exhaust. A particle type with mode diameter < 10 nm was observed after a 623 K (350 °C) catalytic stripper removed all volatile material (as verified experimentally; Figure S2). Therefore, these particles cannot be organics. These particles form a second mode in the non-volatile size distribution (Figure 2) relative to the larger BC mode at 100 nm diameter. It is therefore most likely that this small, non-volatile particle mode represents metal oxides formed by combustion of the lubrication oil. Such particles have been observed previously in diesel-engine exhaust [46]. In support of these conclusions, we note that separate transmission-electron-microscopy measurements of the present samples showed that BC particles had typical aggregate sizes that were much larger than 10 nm (Trivanovic et al., in review) and that the X-ray fluorescence elemental-composition measurements (Table S1) showed that trace metals associated with lubrication oil (Zn, Ca) were the only metals present in the PM with mean concentrations greater than the detection limit. Furthermore, the ratio of these two metals was not statistically different between the two fuels (4.4 ± 1.7 for six LNG-mode samples and 5.3 ± 3 for seven diesel-fuel samples).

4.3. Environmental implications

Our results are relevant to three environmental domains: direct global radiative forcing, BC deposition on snow, and public health.

The radiative-forcing effects of greenhouse gases are often summarized using the global-warming potential metric (GWP) [12]. GWPs are calculated by scaling emission factors up by a constant factor. This is a limited metric for multiple reasons, the most important being that the choice of GWP timescale strongly influences its interpretation [49]. Other reasons include the treatment of emissions as pulsed and the fact that aerosol-climate effects are complex [49, 50, 51]. The technology warming potential (TWP) is a significantly-improved metric [52]. Nevertheless, we calculated the 100-year GWP of CO_2, methane (GWP_{100} of 28 [12]), and BC (GWP_{100} of 680 [51]) using our CO_2 and BC data in combination with the methane emissions from this vessel measured simultaneously with our data and reported by [6]. We found that the GWP of BC was negligible relative to CO_2 and methane, as illustrated by the fact that it is not visible in a plot of these GWPs (Figure S8). This result is due to the much shorter atmospheric lifetime of BC relative to methane and CO_2 [49]. However, the short atmospheric lifetime of BC means that it is deposited onto the planetary surface within approximately 10 days [11], where BC may continue to exert climate forcing, for example by lowering the albedo of snow and ice. These continued climate effects are not taken into account by the GWP.

Figure 7 about here; BC emissions bar chart.

We illustrate the potential snow-albedo impacts of BC emissions in Figure 7, where the emission factors reported in Figure 4 have been weighted according to the ISO 8178 E2 cycle and expressed as emission rates. We have not converted these emission rates into snow albedo reductions as the relationship is complex, being influenced by sublimation, precipitation, atmospheric processing, and snow aging [12, 13, 14]. However, higher emission rates are directly associated with greater snow-albedo reductions. Therefore, our results suggest that the use of NG is favourable over diesel or residual fuels in regions such as the Arctic, where BC deposition may affect climate.

It should be emphasized here that engine tuning and operation may play a large role in the emissions of a particular engine, and that some diesel engines may emit less BC per kWh than observed here. With regard to operation, the operator of the commercial vessel measured in this study has already modified its daily operations such that the engine is not idled at shore; hotel power is rather obtained from shore power. Further

improvements, in collaboration with the engine manufacturer, are expected to be possible, as the present data set reflects the performance of this engine after initial deployment of this relatively-new technology.

With regard to health effects, three issues must be noted. Diesel-fuel exhaust has been statistically associated with lung cancer [56, 57, 58], and mechanistic studies have shown that exhaust toxicity is related to the non-volatile component of the PM [59, 60]. Therefore, the decrease of BC in LNG-mode operation versus diesel-mode operation must correspond to a decrease in certain toxic species. The overall toxicity of the emissions of this engine, considering BC, formaldehyde, and particle number emissions, must be evaluated in future studies.

5. Conclusions

A comprehensive characterization of the particulate matter (PM) emitted by a modern dual-fuel, LNG-powered vessel was performed. The emission factors of organic PM and BC were determined, compared with those of CO_2 and methane, and discussed in terms of the origin of the PM species. Size distributions of total and non-volatile (solid) PM were also reported. Volatile PM had a mode number distribution of approximately 50 nm at idle loads and 10–20 nm at loads above 25%. Non-volatile PM particles were measured with two modes, one above 100 nm and one below 10 nm. Based on TEM evidence, the larger mode was BC; the smaller mode most likely contains metal-oxide particles originating from the combustion of lubrication oil. The larger mode dominated PM mass while the smaller mode contributed significantly to PM number. When the engine was idling at berth, over 99% of the emitted PM mass was organic (volatile) and most likely also originated from lubrication oil. At engine loads above 25%, the majority of the emitted PM mass was BC, most likely originating from the diesel pilot fuel.

The PM measurements were placed in the context of diesel-only mode emissions from the same engine. The BC emissions were over an order of magnitude lower in LNG mode. As a consequence, the snow-and ice-albedo reductions due to BC deposition are predicted to be reduced by at least an order of magnitude in LNG mode. From a GWP perspective, BC emissions are negligible relative to co-emitted methane and CO_2 emissions in both LNG and diesel mode. The long-term (>100-year) GWP of LNG mode emissions was lower than the corresponding diesel mode emissions. The above conclusions do not account for idle emissions, which were over an order of magnitude higher in both cases; idling at low loads should be avoided. In addition, engine emissions may vary substantially between vessels, and emissions-control technology may substantially mitigate the negative impacts of some of the engine emissions.

6. Author contributions

SG conceived and coordinated the study and WM, PL, PK and SG initiated the study. WP, DS, JY, and PK performed the gaseous measurements. UT performed the TEM analysis. SR, DRC, PK, and WP supervised students. JCC performed the particulate measurements, JCC analyzed and interpreted the data with contributions by WP and DS, and wrote the manuscript.

7. Acknowledgements

The authors are very grateful to the vessel operators for their willingness to facilitate this study. We thank Brett Smith (NRC) for assistance with the measurements and logistics. Funding from Transport Canada and the United States Maritime Administration (MARAD) is gratefully acknowledged. Any conclusions or

recommendations expressed in this paper are those of the authors and do not necessarily reflect the views of the vessel operator or the sponsoring agencies.

8. Supporting Information

The online supporting information contains the additional figures mentioned in the main text.

Parameter	Value
Power	4320 kW
Net IMEP	22 bar
Bore and stroke	340 and 400 mm
Displacement	36.3 l/cyl
Speed	720 rpm
Cylinders	9
Intake valves	2
Exhaust valves	2
NG injection	indirect

Table 1: Parameters of the engine studied. IMEP = indicated mean effective pressure.

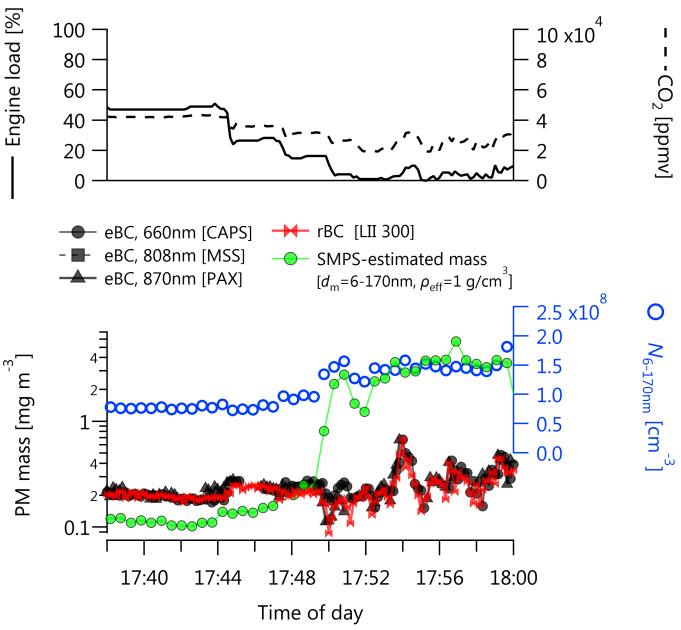

Figure 1: Dilution-corrected time series of BC, CO_2, and particle number concentrations during transition from high load to idle. At loads greater than 20%, the SMPS-estimated mass concentration is smaller than the black carbon mass concentration due to the inaccuracy of the assumed particle shape and density (Section 2). Note the increased variability at idle due to cylinder deactivation. Error bars are omitted for clarity and generally smaller than the data symbols.

Instrument	Abbrev.	DR	Measurand	Reported Quantity
Scanning mobility particle sizer	SMPS	6	Mobility size distributions of nascent and 623 K-denuded particles	$N_{6-170nm}$, $dN/d\log d_{mob}$
AVL 483 Micro Soot Sensor	MSS	6	In-situ aerosol light absorption (photoacoustic)	eBC[a] at 808 nm
ARI CAPS PM_{SSA} monitor	CAPS	6	In-situ aerosol light absorption (extinction-minus-scattering)	eBC[a] at 660 nm
DMT Photoacoustic Extinctiometer	PAX	6	In-situ aerosol light absorption (photoacoustic)	eBC[a] at 870 nm
AVL 415S Smoke Meter	SM	1.0	Light attenuation through PM-laden filter	eBC[a] at 560 nm
Artium LII300	LII	6	Laser-induced incandescence with two-color pyrometry	rBC
Quartz filter samples	-	6	Carbon evolution in inert and oxidizing gases, with optical correction for pyrolysis	EC, OC
Teflon filter samples	-	6	X-ray induced fluorescence	Metal concentrations
Horiba PG350 Gas Analyzer	-	(1.0, 6)[b]	CO, CO_2, NO_x, SO_2	Gas concentrations [ppmv]
LI-COR 850	-	6	CO_2, H_2O	Gas concentrations [ppmv]

Table 2: Instruments used in this study and corresponding principles of measurement. DR = dilution ratio. eBC = equivalent BC, rBC = refractory BC, EC = elemental carbon, OC = organic carbon. [a]All eBC concentrations defined relative to a mass absorption cross section of 7.5 m^2 g at 550 nm, scaled to the measurement wavelength with an Ångström absorption exponent of 1.0 [32]. [b]This instrument was switched between two different lines.

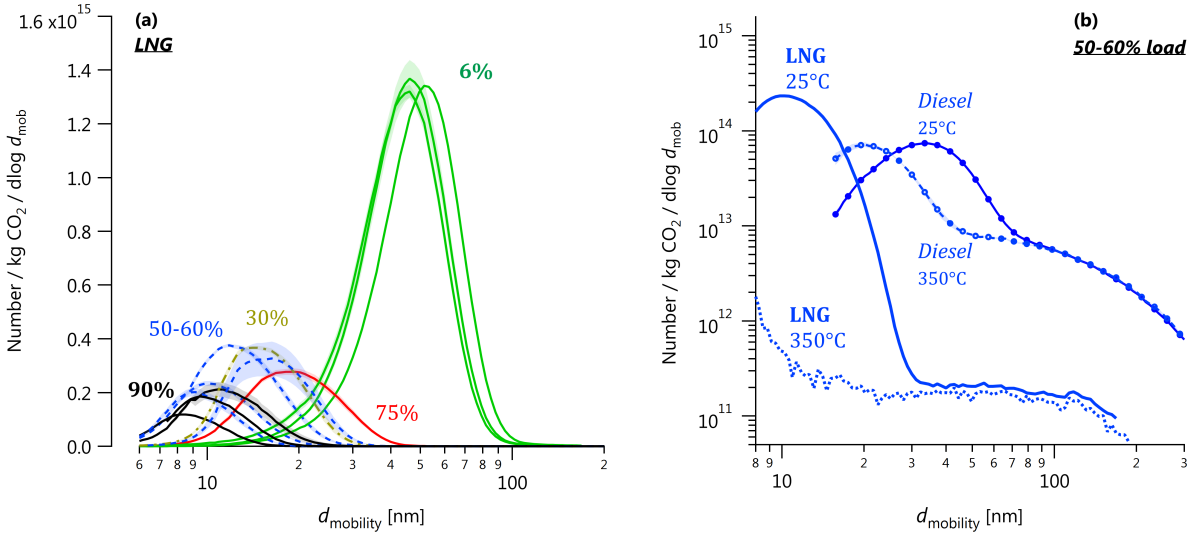

Figure 2: (a) Size distributions as a function of engine load in LNG mode. (b) Size distributions at 50% load for diesel and LNG modes, with and without the removal of volatiles at 623 K by the catalytic stripper.

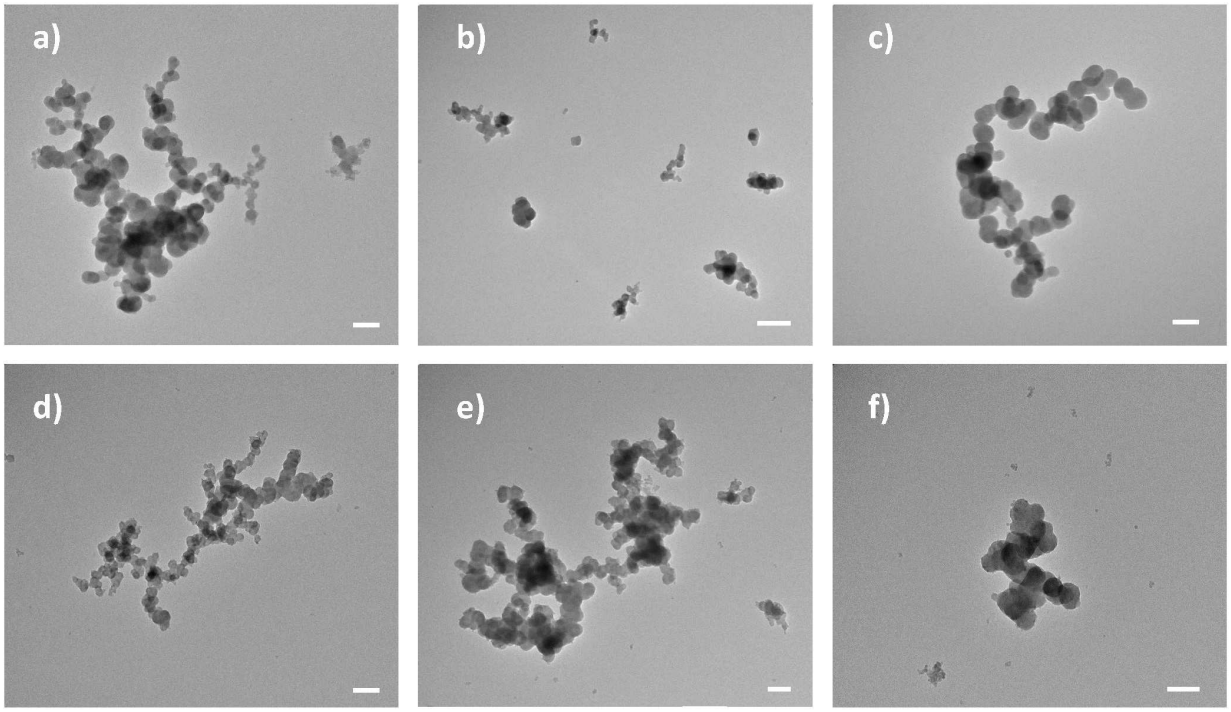

Figure 3: Transmission electron micrographs of representative non-volatile particles sampled when operating in (a–c) LNG mode and (d–f) diesel mode. Note that the organic PM fraction will have evaporated within the vacuum of the microscope. Note also that these images do not represent the extremely-small (< 10 nm) non-volatile particles shown in Figure 2b and discussed in the text.

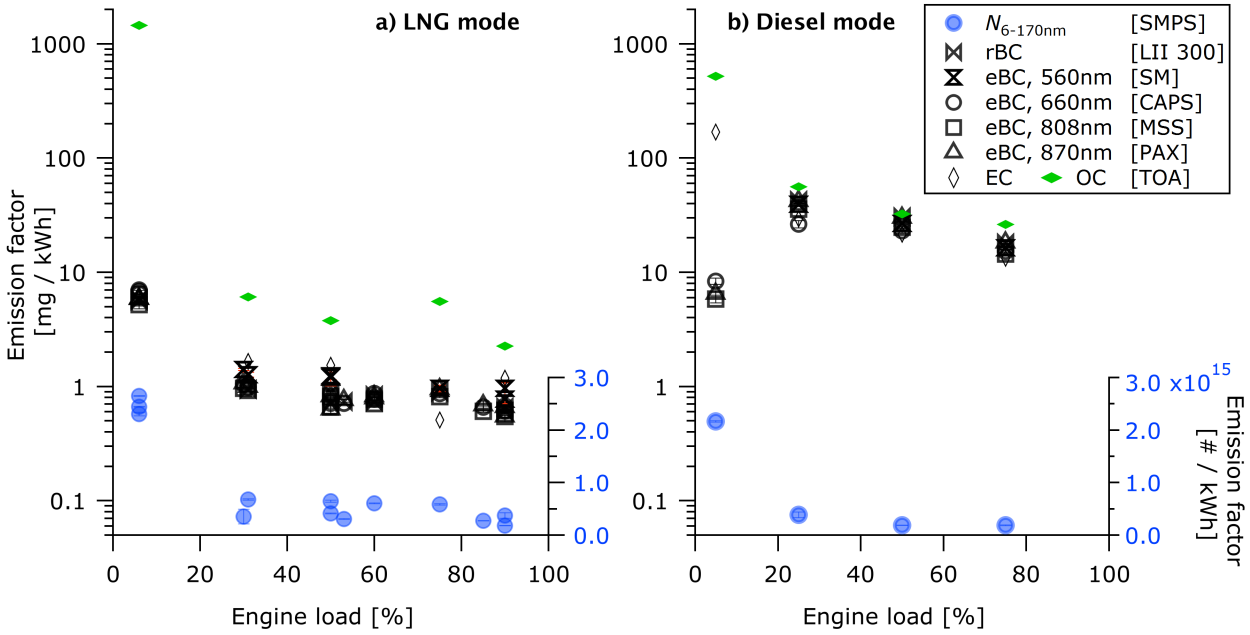

Figure 4: Emission factors per kWh versus load for BC, total PM. (a) LNG mode, (b) diesel mode. Number emission factors measured by SMPS are plotted on the right ordinate; mass emission factors for BC (measured as eBC, rBC, or EC) and OC are plotted on the left ordinate. The positively-biased outlier in EC in panel (b) may be due to high OC concentrations; the corresponding measurement in panel (a) was performed after solvent extraction.

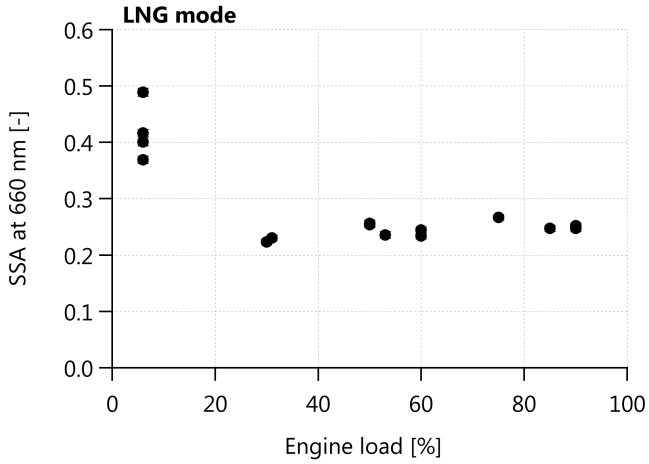

Figure 5: The single-scattering albedo (SSA; ratio of scattering to extinction coefficients) of the aerosol at 660 nm, measured by CAPS PM_{SSA} as a function of engine load. The asymptotic value of ~ 0.2 is typical of BC[37]. Higher values at lower engine loads correspond to increased organic PM concentrations. Error bars are smaller than the data symbols. Corresponding diesel-mode data are not available.

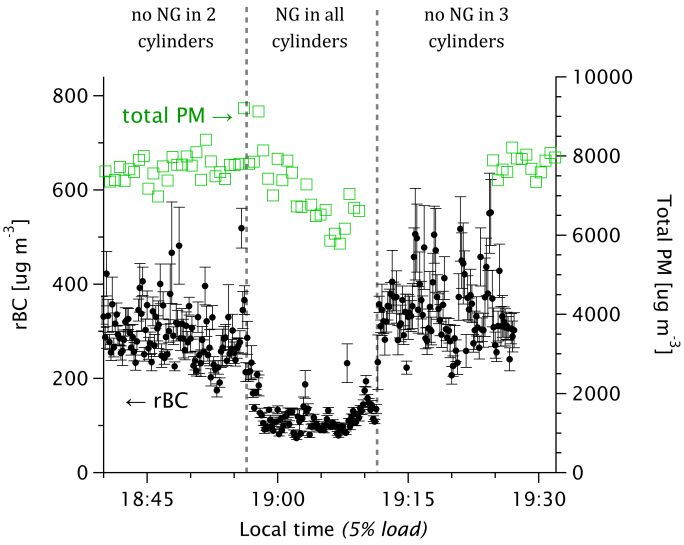

Figure 6: Effect of skipping methane injection on rBC and total PM (estimated by SMPS) concentrations in LNG mode at idle (load 5.4 ± 0.4 %, mean and standard deviation). rBC concentrations were higher and more variable when methane (CH_4) was not injected into the cylinder, suggesting an origin of incomplete pilot-diesel-fuel oxidation. Total PM concentrations decreased only slightly, and with a slow response, when changing injection conditions. Note that the cylinders into which methane was not injected were varied rapidly at each condition.

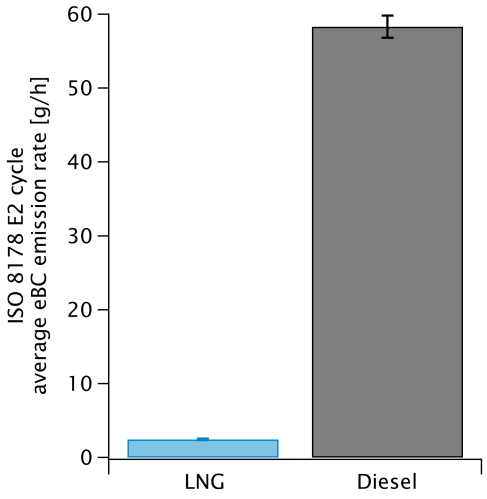

Figure 7: BC emissions averaged over the ISO 8178 E2 Cycle in units of g BC emitted per hour. The E2 cycle weights emissions at loads of $\{25\%, 50\%, 75\%, 100\%\}$ by factors of $\{0.15, 0.15, 0.5, 0.2\}$; we have used data from the nearest available loads (Figure 4) for this calculation. BC deposition onto snow and/or ice is directly related to this emission rate, in addition to depending on atmospheric processing and precipitation.

References

[1] T. Korakianitis, A. Namasivayam, R. Crookes, Natural-gas fueled spark-ignition (SI) and compression-ignition (CI) engine performance and emissions, Progress in Energy and Combustion Science 37 (1) (2011) 89–112. doi:10.1016/j.pecs.2010.04.002.

[2] O. Boucher, D. Randall, P. Artaxo, C. Bretherton, G. Feingold, P. Forster, V. Kerminen, Y. Kondo, H. Liao, U. Lohmann, P. Rasch, S. Satheesh, S. Sherwood, B. Stevens, X. Zhang, Clouds and Aerosols, Cambridge University Press, 2013.
URL http://www.ipcc.ch/report/ar5/wg1/

[3] L. Tartakovsky, M. Sheintuch, Fuel reforming in internal combustion engines, Progress in Energy and Combustion Science 67 (2018) 88–114. doi:10.1016/j.pecs.2018.02.003.

[4] S. Bengtsson, E. Fridell, K. Andersson, Environmental assessment of two pathways towards the use of biofuels in shipping, Energy Policy 44 (2012) 451–463. doi:10.1016/j.enpol.2012.02.030.

[5] S. K. Bengtsson, E. Fridell, K. E. Andersson, Fuels for short sea shipping: A comparative assessment with focus on environmental impact, Proceedings of the Institution of Mechanical Engineers, Part M: Journal of Engineering for the Maritime Environment 228 (1) (2013) 44–54. doi:10.1177/1475090213480349.

[6] D. E. Sommer, M. Yeremi, J. Son, J. C. Corbin, S. Gagné, P. Lobo, J. W. Miller, P. Kirchen, Characterization and reduction of in-use CH4 emissions from a dual fuel marine engine using wavelength modulation spectroscopy, Environmental Science & Technology 53 (5) (2019) 2892–2899. doi:10.1021/acs.est.8b04244.

[7] D. R. Tree, K. I. Svensson, Soot processes in compression ignition engines, Prog. Energy Combust. Sci. 33 (3) (2007) 272–309. doi:10.1016/j.pecs.2006.03.002.

[8] S. Oeder, T. Kanashova, O. Sippula, S. C. Sapcariu, T. Streibel, J. M. Arteaga-Salas, J. Passig, M. Dilger, H.-R. Paur, C. Schlager, S. Mülhopt, S. Diabaté, C. Weiss, B. Stengel, R. Rabe, H. Harndorf, T. Torvela, J. Jokiniemi, M.-R. Hirvonen, C. Schmidt-Weber, C. Traidl-Hoffmann, K. A. BéruBé, A. J. Wlodarczyk, Z. Prytherch, B. Michalke, T. Krebs, A. S. H. Prévôt, M. Kelbg, J. Tiggesbäumker, E. Karg, G. Jakobi, S. Scholtes, J. Schnelle-Kreis, J. Lintelmann, G. Matuschek, M. Sklorz, S. Klingbeil, J. Orasche, P. Richthammer, L. Müller, M. Elsasser, A. Reda, T. Gröger, B. Weggler, T. Schwemer, H. Czech, C. P. Rüger, G. Abbaszade, C. Radischat, K. Hiller, J. T. M. Buters, G. Dittmar, R. Zimmermann, Particulate matter from both heavy fuel oil and diesel fuel shipping emissions show strong biological effects on human lung cells at realistic and comparable in vitro exposure conditions, PLoS One 10 (6) (2015) e0126536. doi:10.1371/journal.pone.0126536.

[9] S. Bengtsson, K. Andersson, E. Fridell, A comparative life cycle assessment of marine fuels, Proceedings of the Institution of Mechanical Engineers, Part M: Journal of Engineering for the Maritime Environment 225 (2) (2011) 97–110. doi:10.1177/1475090211402136.

[10] D. Archer, M. Eby, V. Brovkin, A. Ridgwell, L. Cao, U. Mikolajewicz, K. Caldeira, K. Matsumoto, G. Munhoven, A. Montenegro, K. Tokos, Atmospheric lifetime of fossil fuel carbon dioxide, Annual Review of Earth and Planetary Sciences 37 (1) (2009) 117–134. doi:10.1146/annurev.earth.031208.100206.

[11] D. Jacob, Introduction to atmospheric chemistry, Princeton University Press, Princeton, NJ, USA, 1999.

[12] IPCC, Contribution of Working Group I to the Fourth Assessment Report of the Intergovernmental Panel on Climate Change, Cambridge University Press, United Kingdom and New York, NY, USA, 2007.

[13] R. B. Skeie, T. Berntsen, G. Myhre, C. A. Pedersen, J. Ström, S. Gerland, J. A. Ogren, Black carbon in the atmosphere and snow, from pre-industrial times until present, Atmospheric Chemistry and Physics 11 (14) (2011) 6809–6836. doi:10.5194/acp-11-6809-2011.

[14] S. M. Skiles, M. Flanner, J. M. Cook, M. Dumont, T. H. Painter, Radiative forcing by light-absorbing particles in snow, Nature Climate Change 8 (11) (2018) 964–971. doi:10.1038/s41558-018-0296-5.

[15] P. K. Quinn, A. Stohl, S. Arnold, A. Baklanov, T. Berntsen, J. H. Christensen, S. Eckhardt, M. Flanner, Z. Klimont, Z. Korsholm, K. Kupiainen, J. Langner, K. S. Law, S. Monks, K. von Salzen, M. Sand, J. Schmale, V. Vestreng, AMAP Assessment 2015: Black carbon and ozone as Arctic climate forcers, Arctic Monitoring and Assessment Programme (AMAP), 2015.
URL http://www.amap.no/documents/doc/amap-assessment-2015-black-carbon-and-ozone-as-arctic-climate-1299

[16] M. M. Coggon, A. Sorooshian, Z. Wang, A. R. Metcalf, A. A. Frossard, J. J. Lin, J. S. Craven, A. Nenes, H. H. Jonsson, L. M. Russell, R. C. Flagan, J. H. Seinfeld, Ship impacts on the marine atmosphere: insights into the contribution of shipping emissions to the properties of marine aerosol and clouds, Atmospheric Chemistry and Physics 12 (18) (2012) 8439–8458. doi:10.5194/acp-12-8439-2012.

[17] S. Menon, J. Hansen, L. Nazarenko, Y. Luo, Climate effects of black carbon aerosols in china and india, Science 297 (5590) (2002) 2250–2253.

[18] D. S. Bullock, J. S. Olfert, Size, volatility, and effective density of particulate emissions from a homogeneous charge compression ignition engine using compressed natural gas, Journal of Aerosol Science 75 (2014) 1–8. doi:10.1016/j.jaerosci.2014.04.005.

[19] R. Papagiannakis, D. Hountalas, Combustion and exhaust emission characteristics of a dual fuel compression ignition engine operated with pilot diesel fuel and natural gas, Energy Conversion and Management 45 (18-19) (2004) 2971–2987. doi:10.1016/j.enconman.2004.01.013.

[20] M. Hajbabaei, G. Karavalakis, K. C. Johnson, L. Lee, T. D. Durbin, Impact of natural gas fuel composition on criteria, toxic, and particle emissions from transit buses equipped with lean burn and stoichiometric engines, Energy 62 (2013) 425–434. doi:10.1016/j.energy.2013.09.040.

[21] Å. M. Hallquist, M. Jerksjö, H. Fallgren, J. Westerlund, Å. Sjödin, Particle and gaseous emissions from individual diesel and CNG buses, Atmospheric Chemistry and Physics 13 (10) (2013) 5337–5350. doi:10.5194/acp-13-5337-2013.

[22] J. Li, B. Wu, G. Mao, Research on the performance and emission characteristics of the LNG-diesel marine engine, Journal of Natural Gas Science and Engineering 27 (2015) 945–954. doi:10.1016/j.jngse.2015.09.036.

[23] E. R. Jayaratne, N. K. Meyer, Z. D. Ristovski, L. Morawska, Volatile properties of particles emitted by compressed natural gas and diesel buses during steady-state and transient driving modes, Environmental Science & Technology 46 (1) (2011) 196–203. doi:10.1021/es2026856.

[24] M. Anderson, K. Salo, E. Fridell, Particle- and gaseous emissions from an LNG powered ship, Environmental Science & Technology 49 (20) (2015) 12568–12575. doi:10.1021/acs.est.5b02678.

[25] L. Turrio-Baldassarri, C. L. Battistelli, L. Conti, R. Crebelli, B. D. Berardis, A. L. Iamiceli, M. Gambino, S. Iannaccone, Evaluation of emission toxicity of urban bus engines: Compressed natural gas and comparison with liquid fuels, Science of The Total Environment 355 (1-3) (2006) 64–77. doi:10.1016/j.scitotenv.2005.02.037.

[26] N. R. Gysel, W. A. Welch, K. Johnson, W. Miller, D. R. Cocker, Detailed analysis of criteria and particle emissions from a very large crude carrier using a novel ECA fuel, Environmental Science & Technology 51 (3) (2017) 1868–1875. doi:10.1021/acs.est.6b02577.

[27] F. Cavalli, M. Viana, K. E. Yttri, J. Genberg, J.-P. Putaud, Toward a standardised thermal-optical protocol for measuring atmospheric organic and elemental carbon: the EUSAAR protocol, Atmospheric Measurement Techniques 3 (1) (2010) 79–89. doi:10.5194/amt-3-79-2010.

[28] A. Miller, G. Frey, G. King, C. Sunderman, A handheld electrostatic precipitator for sampling airborne particles and nanoparticles, Aerosol Science and Technology 44 (6) (2010) 417–427. doi:10.1080/02786821003692063.

[29] A. Petzold, J. Ogren, M. Fiebig, P. Laj, S.-M. Li, U. Baltensperger, T. Holzer-Popp, S. Kinne, G. Pappalardo, N. Sugimoto, C. Wehrli, A. Wiedensohler, X.-Y. Zhang, Recommendations for the interpretation of "black carbon" measurements, Atmos. Chem. Phys. 13 (16) (2013) 8365–8379. doi:10.5194/acp-13-8365-2013.

[30] T. C. Bond, S. J. Doherty, D. W. Fahey, P. M. Forster, T. Berntsen, B. J. DeAngelo, M. G. Flanner, S. Ghan, B. Kärcher, D. Koch, S. Kinne, Y. Kondo, P. K. Quinn, M. C. Sarofim, M. G. Schultz, M. Schulz, C. Venkataraman, H. Zhang, S. Zhang, N. Bellouin, S. K. Guttikunda, P. K. Hopke, M. Z. Jacobson, J. W. Kaiser, Z. Klimont, U. Lohmann, J. P. Schwarz, D. Shindell, T. Storelvmo, S. G. Warren, C. S. Zender, Bounding the role of black carbon in the climate system: A scientific assessment, J. Geophys. Res. Atmos. 118 (2013) 5380–5552. doi:10.1002/jgrd.50171.

[31] J. C. Corbin, H. Czech, D. Massabo, F. Buatier de Mongeot, G. Jakobi, F. Liu, P. Lobo, C. Mennucci, A. A. Mensah, J. Orasche, S. M. Pieber, A. S. H. Prévôt, B. Stengel, L. L. Tay, M. Zanatta, R. Zimmermann, I. El Haddad, M. Gysel-Beer, Refractory, infrared-absorbing carbon in ship exhaust from heavy fuel oil combustion, in press at npj Atmospheric and Climate Sciencedoi:10.1038/s41612-019-0069-5.

[32] H. Moosmüller, R. Chakrabarty, W. Arnott, Aerosol light absorption and its measurement: A review, Journal of Quantitative Spectroscopy and Radiative Transfer 110 (11) (2009) 844–878. doi:10.1016/j.jqsrt.2009.02.035.

[33] T. Nakayama, H. Suzuki, S. Kagamitani, Y. Ikeda, A. Uchiyama, Y. Matsumi, Characterization of a three wavelength photoacoustic soot spectrometer (PASS-3) and a photoacoustic extinctiometer (PAX), Journal of the Meteorological Society of Japan. Ser. II 93 (2) (2015) 285–308. doi:10.2151/jmsj.2015-016.

[34] T. B. Onasch, P. Massoli, P. L. Kebabian, F. B. Hills, F. W. Bacon, A. Freedman, Single scattering albedo monitor for airborne particulates, Aerosol Sci. Technol. 49 (4) (2015) 267–279. doi:10.1080/02786826.2015.1022248.

[35] W. Schindler, C. Haisch, H. A. Beck, R. Niessner, E. Jacob, D. Rothe, A photoacoustic sensor system for time resolved quantification of diesel soot emissions, in: SAE Technical Paper Series, SAE International, 2004. doi:10.4271/2004-01-0968.

[36] W. F. Northrop, S. V. Bohac, J.-Y. Chin, D. N. Assanis, Comparison of filter smoke number and elemental carbon mass from partially premixed low temperature combustion in a direct-injection diesel engine, Journal of Engineering for Gas Turbines and Power 133 (10) (2011) 102804. doi:10.1115/1.4002918.

[37] T. C. Bond, R. W. Bergstrom, Light absorption by carbonaceous particles: An investigative review, Aerosol Sci. Technol. 40 (1) (2006) 27–67. doi:10.1080/02786820500421521.

[38] H. Moosmüller, W. P. Arnott, Particle optics in the rayleigh regime, Journal of the Air & Waste Management Association 59 (9) (2009) 1028–1031. doi:10.3155/1047-3289.59.9.1028.

[39] D. R. Snelling, G. J. Smallwood, F. Liu, Ömer L. Gülder, W. D. Bachalo, A calibration-independent laser-induced incandescence technique for soot measurement by detecting absolute light intensity, Applied Optics 44 (31) (2005) 6773. doi:10.1364/ao.44.006773.

[40] H. Schmid, L. Laskus, H. J. Abraham, U. Baltensperger, V. Lavanchy, M. Bizjak, P. Burba, H. Cachier, D. Crow, J. Chow, T. Gnauk, A. AEven, H. M. ten Brink, K.-P. Giesen, R. Hitzenberger, C. Hueglin, W. Maenhaut, C. Pio, A. Carvalho, J.-P. Putaud, D. Toom-Sauntry, H. Puxbaum, Results of the "carbon conference" international aerosol carbon round robin test stage i, Atmospheric Environment 35 (12) (2001) 2111–2121. doi:10.1016/s1352-2310(00)00493-3.

[41] S.-L. von der Weiden, F. Drewnick, S. Borrmann, Particle loss calculator – a new software tool for the assessment of the performance of aerosol inlet systems, Atmospheric Measurement Techniques 2 (2) (2009) 479–494. doi:10.5194/amt-2-479-2009.

[42] P. Kulkarni, P. A. Baron, K. Willeke, Aerosol measurement: principles, techniques, and applications, John Wiley & Sons, 2011.

[43] M. D. Wilson, D. M. Rocke, B. Durbin, H. D. Kahn, Detection limits and goodness-of-fit measures for the two-component model of chemical analytical error, Anal. Chim. Acta 509 (2) (2004) 197–208. doi:10.1016/j.aca.2003.12.047.

[44] K. Park, F. Cao, D. B. Kittelson, P. H. McMurry, Relationship between particle mass and mobility for diesel exhaust particles, Environmental Science & Technology 37 (3) (2003) 577–583. doi:10.1021/es025960v.

[45] M. Gysel, M. Laborde, A. A. Mensah, J. C. Corbin, A. Keller, J. Kim, A. Petzold, B. Sierau, Technical note: The single particle soot photometer fails to reliably detect palas soot nanoparticles, Atmos. Meas. Tech. 5. doi:10.5194/amt-5-3099-2012.

[46] A. C. Mayer, A. Ulrich, J. Czerwinski, J. J. Mooney, Metal-oxide particles in combustion engine exhaust, in: SAE Technical Paper Series, no. 2010-01-0792, SAE International, 2010. doi:10.4271/2010-01-0792.

[47] E. M. Lipsky, A. L. Robinson, Effects of dilution on fine particle mass and partitioning of semivolatile organics in diesel exhaust and wood smoke, Environ. Sci. Technol. 40 (1) (2006) 155–162. doi:10.1021/es050319p.

[48] J. Swanson, D. Kittelson, Factors influencing mass collected during 2007 diesel PM filter sampling, SAE International Journal of Fuels and Lubricants 2 (1) (2009) 718–729. doi:10.4271/2009-01-1517.

[49] R. Pierrehumbert, Short-lived climate pollution, Annual Review of Earth and Planetary Sciences 42 (1) (2014) 341–379. doi:10.1146/annurev-earth-060313-054843.

[50] M. R. Allen, K. P. Shine, J. S. Fuglestvedt, R. J. Millar, M. Cain, D. J. Frame, A. H. Macey, A solution to the misrepresentations of CO2-equivalent emissions of short-lived climate pollutants under ambitious mitigation, npj Climate and Atmospheric Science 1 (1). doi:10.1038/s41612-018-0026-8.

[51] T. C. Bond, H. Sun, Can reducing black carbon emissions counteract global warming?, Environmental Science & Technology 39 (16) (2005) 5921–5926. doi:10.1021/es0480421.

[52] H. Thomson, J. J. Corbett, J. J. Winebrake, Natural gas as a marine fuel, Energy Policy 87 (2015) 153–167. doi:10.1016/j.enpol.2015.08.027.

[56] L. Benbrahim-Tallaa, R. A. Baan, Y. Grosse, B. Lauby-Secretan, F. El Ghissassi, V. Bouvard, N. Guha, D. Loomis, K. Straif, Carcinogenicity of diesel-engine and gasoline-engine exhausts and some nitroarenes, The Lancet Oncology 13 (7) (2012) 663–664. doi:10.1016/S1470-2045(12)70280-2.

[57] D. Pallapies, D. Taeger, F. Bochmann, P. Morfeld, Comment: Carcinogenicity of diesel-engine exhaust (de), Arch. Toxicol. 87 (3) (2013) 547–549. doi:10.1007/s00204-012-0955-7.

[58] Y. Sun, F. Bochmann, A. Nold, M. Mattenklott, Diesel exhaust exposure and the risk of lung cancer–a review of the epidemiological evidence, Int. J. Environ. Res. Public. Health 11 (2) (2014) 1312–1340. doi:10.3390/ijerph110201312.

[59] C.-J. G. Pan, D. A. Schmitz, A. K. Cho, J. Froines, J. M. Fukuto, Inherent redox properties of diesel exhaust particles: catalysis of the generation of reactive oxygen species by biological reductants, Toxicol. Sci. 81 (1) (2004) 225–232. doi:10.1093/toxsci/kfh199.

[60] R. D. McWhinney, K. Badali, J. Liggio, S.-M. Li, J. P. Abbatt, Filterable redox cycling activity: a comparison between diesel exhaust particles and secondary organic aerosol constituents, Environ. Sci. Technol. 47 (7) (2013) 3362–3369. doi:10.1021/es304676x.

[61] B. J. Turpin, H.-J. Lim, Species contributions to pm2.5 mass concentrations: Revisiting common assumptions for estimating organic mass, Aerosol Sci. Technol. 35 (1) (2001) 602–610. doi:10.1080/02786820119445.

[54] R. A. Alvarez, D. Zavala-Araiza, D. R. Lyon, D. T. Allen, Z. R. Barkley, A. R. Brandt, K. J. Davis, S. C. Herndon, D. J. Jacob, A. Karion, E. A. Kort, B. K. Lamb, T. Lauvaux, J. D. Maasakkers, A. J. Marchese, M. Omara, S. W. Pacala, J. Peischl, A. L. Robinson, P. B. Shepson, C. Sweeney, A. Townsend-Small,

S. C. Wofsy, S. P. Hamburg, Assessment of methane emissions from the u.s. oil and gas supply chain, Science (2018) eaar7204doi:10.1126/science.aar7204.